XLVI CILAMCE
VITÓRIA - ES - BRAZIL - 2025
XLVI IBERO-LATIN AMERICAN CONGRESS ON COMPUTATIONAL METHODS IN ENGENEERING

# Computational Fluid Dynamics Simulations for Hemodynamic Analysis of Coronary Artery Disease

Juan J. Zuluaga Patiño[1], Jose A. Guerrero-Vargas[1].

[1] *School of Sciences and Engineering, Universidad del Rosario*
*Carrera 6 No 12C-16, Zip-Code 111711, Bogotá, D.C., Colombia*
*juanjo.zuluaga@urosario.edu.co, joseal.guerrero@urosario.edu.co*

**Abstract.** Coronary artery disease (CAD) remains a major cause of mortality worldwide, yet the link between arterial morphology and hemodynamic disturbances is not fully understood. This study aims to address this through computational fluid dynamics simulations of blood flow in coronary arteries with varying degrees of stenosis. Using a custom finite element solver for the Navier–Stokes equations, velocity, pressure, wall shear stress, and vorticity are evaluated. Results show that increased stenosis severity leads to higher peak velocities, elevated wall shear stress, and larger recirculation zones downstream, with a transitional unsteady flow appearing in severe constrictions. These findings highlight the strong influence of geometric narrowing on local hemodynamics, offering insights relevant to plaque development and disease progression.

**Keywords:** Computational fluid dynamics, Coronary artery disease, Incompressible Navier–Stokes.

## 1 Introduction

Cardiovascular diseases remain the leading cause of mortality worldwide, accounting for nearly one-third of all deaths according to the World Health Organization [1], with coronary artery disease (CAD) being one of the most prevalent and severe forms. This condition arises from the buildup of atherosclerotic plaques that narrow the coronary arteries and disturb local hemodynamics, increasing the risk of ischemic events. According to Ku [2], blood flow patterns play a crucial role in atherosclerosis progression, with regions of low and oscillatory wall shear stress (WSS) being particularly prone to plaque deposition. Malek [3] further emphasized that such hemodynamic disturbances modulate endothelial function and vascular remodeling.

Computational fluid dynamics (CFD) has become a valuable tool for analyzing these flow-related phenomena in realistic and idealized vascular geometries. Steinman and Taylor [4] demonstrated how CFD enables quantitative analysis of large-artery hemodynamics. Perktold et al. [5] studied pulsatile flow in realistic coronary bifurcations, showing that curvature and branching generate complex shear patterns that may promote plaque localization. Similarly, Tu and Deville [6] analyzed flow through idealized stenotic arteries, reporting that increasing constriction severity amplifies velocity, pressure drop, and WSS gradients. Collectively, these studies advanced understanding of the mechanical factors driving CAD.

Despite these advances, how stenosis geometry modulates local hemodynamics remains not fully understood. Most existing studies focus on three-dimensional, patient-specific reconstructions which are computationally expensive and difficult to validate. Simplified two-dimensional or rigid-wall models remain valuable for isolating geometric effects and validating implementations. However, most prior research has relied on commercial software or proprietary algorithms, limiting reproducibility and accessibility.

The present work implements and validates a stabilized finite element solver for the incompressible Navier–Stokes equations using the open-source FEniCSx platform. The solver is validated and applied to analyze how varying stenosis severity influences velocity, pressure, and WSS in coronary-like geometries.

## 2 Methodology

The incompressible Navier–Stokes equations describe the motion of viscous fluids that do not undergo density variations. In particular, they model the conservation of momentum and mass for a Newtonian fluid and are widely used in the study of biological flows, such as blood flow, where incompressibility is a valid approximation under certain physiological conditions as discussed by Ku [2]. Although blood is a non-Newtonian fluid, in large arteries such as the coronaries, shear rates are sufficiently high that PoojaJhunjhunwala [7] showed that a Newtonian blood model provides a good approximation.

$$\rho\left(\frac{\partial u}{\partial t} + u \cdot \nabla u\right) = \nabla \cdot \sigma(u,p) + f. \tag{1a}$$

$$\nabla \cdot u = 0. \tag{1b}$$

$$\sigma(u,p) = \mu(\nabla u + (\nabla u)^T) - pI. \tag{1c}$$

Where $u : \mathbb{R}^d \times \mathbb{R}_+ \to \mathbb{R}^d$ and $p : \mathbb{R}^d \times \mathbb{R}_+ \to \mathbb{R}$ correspond to velocity and pressure, respectively, as functions of space and time. $d \in \{2,3\}$ is the spatial dimension, $\rho$ is the fluid density, $\mu$ is the fluid dynamic viscosity and $f : \mathbb{R}^d \to \mathbb{R}^d$ is an external force applied to the system. Equations (1a) and (1b), together with Dirichlet conditions $g(t)$, an initial condition $u_0$, and a geometric domain $\Omega \in \mathbb{R}^d$ conform the strong problem formulation.

$$u(x,0) = u_0(x) \tag{2a}$$

$$u(x,t) = g(t) \quad \forall x \in \Gamma_D \tag{2b}$$

Where $\Gamma_D \subset \Omega$ is the part of the boundary where Dirichlet conditions are prescribed.

To solve this problem using the finite element method, it is transformed into its variational formulation, also known as the weak formulation. This is achieved by multiplying the equations by suitable test functions and integrating; after applying integration by parts on the stress term, a system with derivatives of lower order than the original one is obtained. We define the forms $a$ and $b$ corresponding to the momentum and continuity weak equations, respectively:

$$a(u,p,v) = \int_\Omega \rho \frac{\partial u}{\partial t} \cdot v \, dx + \int_\Omega \rho u \cdot \nabla u \cdot v \, dx + \int_\Omega \sigma(u,p) \cdot \nabla v \, dx - \int_\Omega (\sigma(u,p) \cdot n) \cdot v \, ds - \int_\Omega f \cdot v \, dx, \tag{3}$$

$$b(u,q) = \int_\Omega \nabla \cdot u \cdot q \, dx. \tag{4}$$

Then, the weak formulation of the problem is: find $u \in V$ and $p \in Q$ such that $a(u,p,v) = 0$ and $b(u,q) = 0$ for all $v \in V$ and $q \in Q$. Where $V = [H^1(\Omega)]^d$ and $Q = L^2(\Omega)$.

The implemented scheme uses a fully implicit midpoint discretization, which is a second-order accurate, A-stable Runge–Kutta method. According to Sanderse [8], it is exactly energy-conserving, however, it is not L-stable, so stiff problems could result in an oscillatory solution.

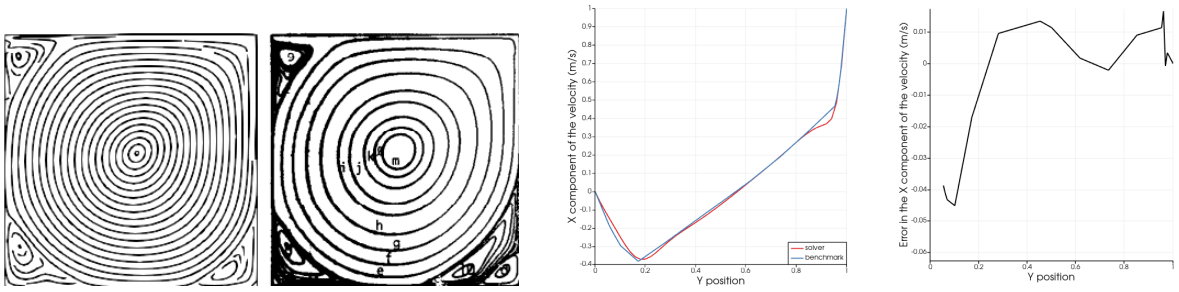
To improve numerical stability and enable the use of the pair $P_1/P_1$ for velocity and pressure spaces, three stabilization terms introduced by Brooks and Hughes [9] and Hughes et al. [10, 11] were incorporated into the weak form. Specifically, SUPG (Streamline-Upwind Petrov–Galerkin) was used to mitigate oscillations in convection-dominated flows , PSPG (Pressure-Stabilizing Petrov–Galerkin) to stabilize the pressure field and bypass the LBB condition, and LSIC (Least-Squares Incompressibility Constraint) to enhance mass conservation and improve the conditioning of the continuity equation. The nonlinear system of equations arising from the weak form is then solved with the Newton method.

The linear system for the update $J(x_k)\Delta x_k = -F(x_k)$ exhibits a saddle-point structure, typical of Stokes and Navier–Stokes problems, with blocks that couple velocity and pressure. To solve it efficiently, a preconditioner based on the Schur complement is used. Different Krylov methods are used for each block of the preconditioned

system. In the simulations considered, the number of Newton iterations remained low, with the residual falling below $10^{-10}$ in 2-4 iterations.

To validate the implementation, the 2D lid-driven cavity flow benchmark was executed, the streamline plots and the velocity point values were compared with the results of Ghia et al. [12], the comparison is shown in Fig. 1.

A mesh sensitivity test varying the number of cells from about 2,000 to 9,000 showed velocity magnitude variations below 1%, indicating mesh convergence.




(a) (b) (c)

Figure 1. Comparison with the lid-driven cavity flow benchmark: (a) Streamline plots at $Re = 10000$ on the left is from the present solver, on the right is from Ghia et al. [12]. (b) Error of the X component of the velocity. (c) Comparison of the X component of the velocity along the line $x = 0.5$ against data from Ghia et al. [12]

## 3 Results

To explore the effect of varying stenosis severity on local hemodynamics, we simulated flow in three symmetric two-dimensional geometries with progressive constriction severity, modeled as local reductions in channel height to 25%, 50%, and 75%. Poiseuille profile is prescribed at inlet, zero pressure at outlet.

In the 25% obstruction case, the flow remains laminar and reaches steady state. No recirculation zones are observed due to the low slope and wide shape of the narrowing. As shown in Fig. 2, the parabolic velocity profile is maintained upstream, increasing inside the stenosis, reaching a sharp peak before gradually returning to pre-stenotic levels. This is illustrated in Fig. 3a, where velocity along the centerline is plotted for each geometry.

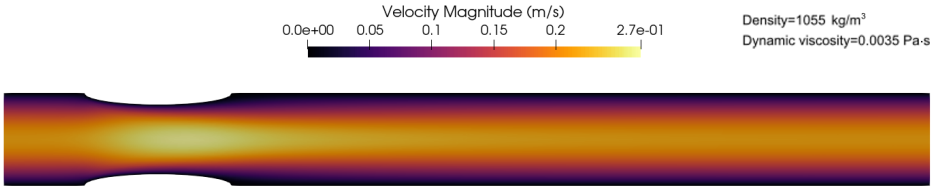
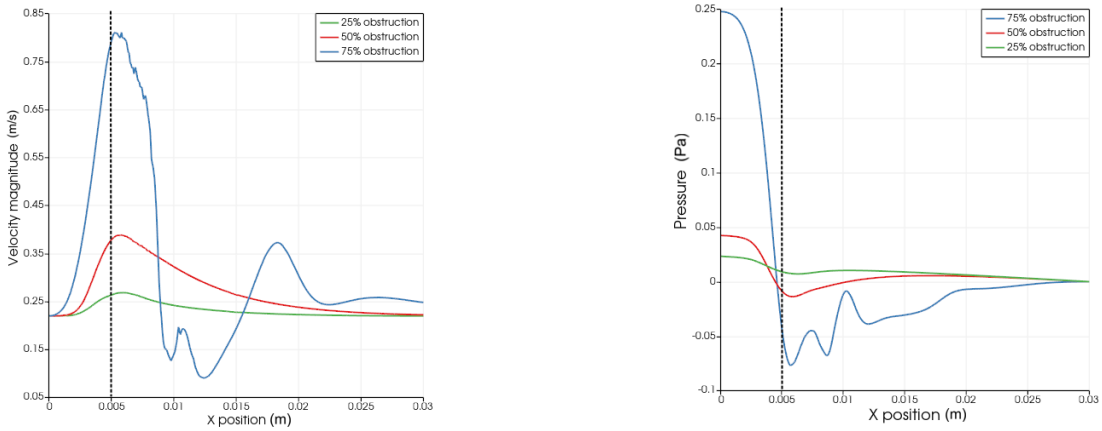



Figure 2. Velocity magnitude field for the 25% stenosis case.

In the 50% case, the flow also remains laminar and stationary, but two symmetric recirculation zones appear immediately downstream of the stenosis, as can be seen in Fig. 4. The velocity peak in the stenosis is higher and sustained over a longer region. On the other hand, in the 75% case, the flow exhibits transitional behavior and does not reach a steady state. Instead, a periodic unsteady regime is observed, where the velocity pulses after the stenosis. Two asymmetric recirculation zones develop initially, followed by a third zone farther downstream due to the curved trajectory of the jet. Figure 5 shows the velocity field.

As shown in Fig. 3b, for all three cases, pressure decreases sharply at the entrance of the stenosis, reaching a minimum shortly downstream of the narrowest section it then rises slowly, to reach zero at the outlet. This behavior is more pronounced as the degree of constriction increases.

All cases show peak wall shear stress at the entrance and within the stenosis region. The magnitude of this peak increases with obstruction severity. After stenosis, the WSS almost reaches zero. For the 25% and 50% obstruction cases the WSS steadily recovers along the post-stenotic region, until reaching pre-stenotic levels. For the 75% case, after the stenosis, the WSS distribution has an oscillatory pattern that follows the curved trajectory




(a) Velocity. (b) Pressure.

Figure 3. Centerline (a) velocity and (b) pressure profiles for all stenosis levels. The dotted line indicates the x position of the narrowest section.

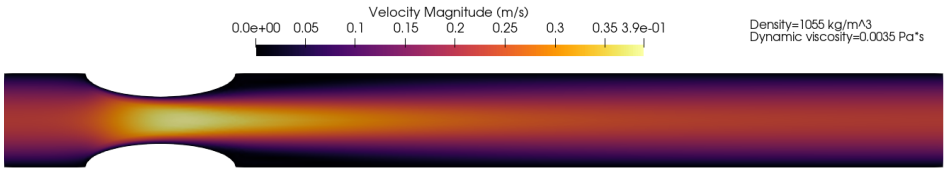



Figure 4. Velocity magnitude field and surface LIC for the 50% stenosis case.

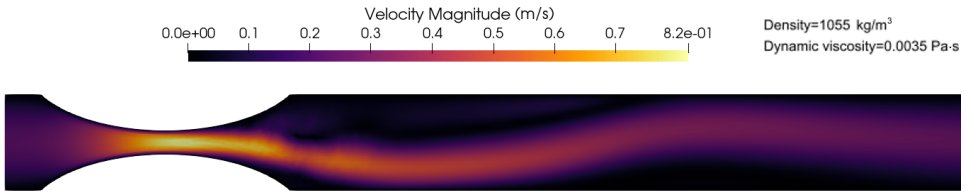
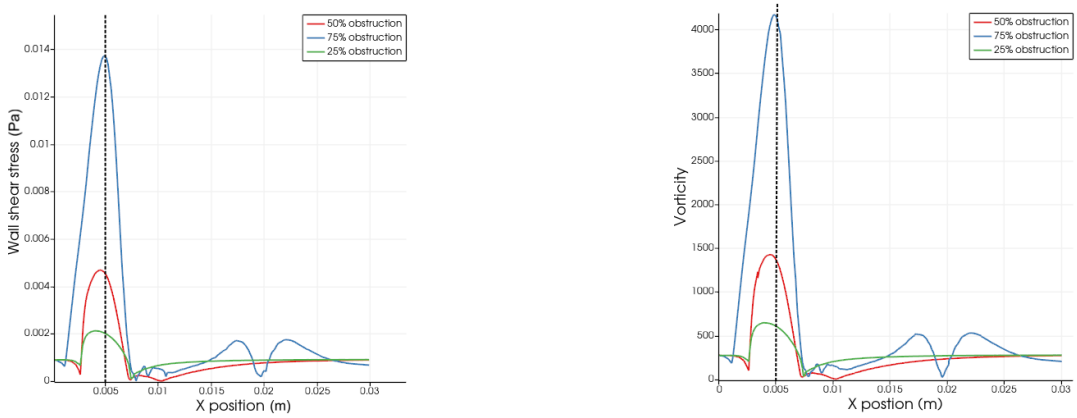



Figure 5. Velocity magnitude field for the 75% stenosis case.




(a) Wall shear stress. (b) Vorticity.

Figure 6. Profiles of (a) wall shear stress along the upper wall and (b) vorticity along the centerline for all stenosis levels. The dotted line indicates the x position of the narrowest section.

of the flow. Figure 6a shows the WSS distribution along the top wall; the bottom wall distribution is similar. Note

that for the 75% case the WSS rises earlier and reaches minimum later, that is because for this case the stenosis is wider, however for all cases WSS starts rising and reaches minimum at the entrance and exit respectively.

The vorticity field shows high magnitudes near walls, particularly at the entrance and midsection of the stenosis. Its overall magnitude increases with obstruction severity. Vorticity distribution along the top wall is shown in Fig. 6b.

## 4 Conclusions

The simulations show that as the severity of the stenosis increases, the maximum velocity and the wall shear stress within the constriction raise sharply, while larger and more persistent recirculation zones form downstream. Under the assessed conditions, in the 25% and 50% cases, low–shear regions are persistent, whereas the 75% case exhibits transitional, oscillatory flow, with low and high WSS regions. According to Moorejr et al. [13], these conditions correlate with plaque development in the region. These results reinforce the idea that geometric narrowing critically alters local hemodynamics in ways known to influence disease development. The main contribution of this work is the implementation and validation of a stabilized finite element solver in FEniCSx for the incompressible Navier–Stokes equations, which is then applied to explore hemodynamic effects of arterial stenosis.

**Acknowledgements.** The authors thank Professor Sebastián Jaramillo Isaza for reviewing the work and providing valuable feedback.

**Authorship statement.** The authors hereby confirm that they are the sole liable persons responsible for the authorship of this work, and that all material that has been herein included as part of the present paper is either the property (and authorship) of the authors, or has the permission of the owners to be included here.

## References

[1] World Health Organization. Cardiovascular diseases (CVDs), 2021.
[2] D. N. Ku. BLOOD FLOW IN ARTERIES. *Annual Review of Fluid Mechanics*, vol. 29, n. 1, pp. 399–434, 1997.
[3] A. M. Malek. Hemodynamic Shear Stress and Its Role in Atherosclerosis. *JAMA*, vol. 282, n. 21, pp. 2035, 1999.
[4] D. A. Steinman and C. A. Taylor. Flow Imaging and Computing: Large Artery Hemodynamics. *Annals of Biomedical Engineering*, vol. 33, n. 12, pp. 1704–1709, 2005.
[5] K. Perktold, M. Hofer, G. Rappitsch, M. Loew, B. Kuban, and M. Friedman. Validated computation of physiologic flow in a realistic coronary artery branch. *Journal of Biomechanics*, vol. 31, n. 3, pp. 217–228, 1997.
[6] C. Tu and M. Deville. Pulsatile flow of non-Newtonian fluids through arterial stenoses. *Journal of Biomechanics*, vol. 29, n. 7, pp. 899–908, 1996.
[7] S. T. P.M. Padole. PoojaJhunjhunwala. Non-newtonian blood flow in left coronary arteries with varying stenosis: A comparative study. *Molecular & Cellular Biomechanics*, vol. 13, n. 1, pp. 1–21, 2016.
[8] B. Sanderse. Energy-conserving Runge–Kutta methods for the incompressible Navier–Stokes equations. *Journal of Computational Physics*, vol. 233, pp. 100–131, 2013.
[9] A. N. Brooks and T. J. Hughes. Streamline upwind/Petrov-Galerkin formulations for convection dominated flows with particular emphasis on the incompressible Navier-Stokes equations. *Computer Methods in Applied Mechanics and Engineering*, vol. 32, n. 1-3, pp. 199–259, 1982.
[10] T. J. Hughes, L. P. Franca, and G. M. Hulbert. A new finite element formulation for computational fluid dynamics: VIII. The galerkin/least-squares method for advective-diffusive equations. *Computer Methods in Applied Mechanics and Engineering*, vol. 73, n. 2, pp. 173–189, 1989.
[11] T. J. Hughes, L. P. Franca, and M. Balestra. A new finite element formulation for computational fluid dynamics: V. Circumventing the babuška-brezzi condition: a stable Petrov-Galerkin formulation of the stokes problem accommodating equal-order interpolations. *Computer Methods in Applied Mechanics and Engineering*, vol. 59, n. 1, pp. 85–99, 1986.
[12] U. Ghia, K. Ghia, and C. Shin. High-Re solutions for incompressible flow using the Navier-Stokes equations and a multigrid method. *Journal of Computational Physics*, vol. 48, n. 3, pp. 387–411, 1982.
[13] J. Moorejr, C. Xu, S. Glagov, C. Zarins, and D. Ku. Fluid wall shear stress measurements in a model of the human abdominal aorta: oscillatory behavior and relationship to atherosclerosis. *Atherosclerosis*, vol. 110, n. 2, pp. 225–240, 1994.